Three dimensional CFD simulation of LPG tanks exposed to partially engulfing pool fires

Three dimensional CFD simulation of LPG tanks exposed to partially engulfing pool fires

Giordano Emrys SCARPONI[a,*], Gabriele LANDUCCI[b], Albrecht Micheal BIRK[c], Valerio COZZANI[a]

[a] LISES - Department of Civil, Chemical, Environmental and Material Engineering, Alma Mater Studiorum – University of Bologna, via Terracini 28, 40131, Bologna (Italy)

[b] Department of Civil and Industrial Engineering, University of Pisa, Largo Lucio Lazzarino 2, 56126, Pisa (Italy)

[c] Dept. of Mechanical and Materials Engineering, McLaughlin Hall, Queen's University, Kingston, ON, Canada K7L 3N6

(*) Author to whom correspondence should be addressed:
tel. (+39)-051-2090250;
e-mail: giordano.scarponi@unibo.it

Submitted for publication in:
PROCESS SAFETY AND ENVIRONMENTAL PROTECTION

ABSTRACT

The availability of accurate and robust models for the prediction of the behavior of pressurized tanks under fire exposure is a key requirement to improve the design of fire protection systems. Most of the models present in the literature take into consideration fully engulfing pool fire scenarios only. In the present study, a CFD modelling approach previously validated against full engulfing pool fires tests is used to simulate partial engulfment conditions. The model allowed analyzing local flow field promoting thermal stratification, which in turn drives internal pressurization of the tank. Comparison with fire test results shows good agreement with experimental measurements both in terms of temperature and pressurization curves. The results obtained represent a valuable source of information to support risk management, the planning of emergency response and improve fire protection systems design.

Keywords

LPG tank, Partial engulfment, Pressure vessel exposed to fire, Thermal stratification, CFD modeling.

1 Introduction

The possible occurrence of accidental fires involving tanks for the storage or the transportation of gases liquefied under pressure, such as liquefied petroleum gas (LPG), represents a critical safety issue in the process industry and in the management of infrastructures for the transportation of goods, as highways and railways. The heat load generated by the fire may induce the vessel failure, which can result in extremely dangerous events such as Boiling Liquid Expanding Vapor Explosion (BLEVE), fireball and missiles projection (Leslie and Birk, 1991; Mcdevitt, 1990; Moodie et al., 1985). A huge number of such accidents is reported in the literature (e.g. see the review of Abbasi and Abbasi, 2007), with severe impact on the population, as evident from the recent accident that took place on the Bologna highway in Italy (Malm, 2018) and from the Lac-Megantic accident in Canada (U.S. Department of Transportation, 2013).

The prevention of these accidents requires a continuous improvement of codes and standards for design, operation and maintenance of tanks and thermal protection systems (Bradley et al., 2021; Di Padova et al., 2011; Tugnoli et al., 2012). This entails the understanding of the phenomena characterizing the behavior of fluids liquefied under pressure when exposed to intense fires inside tanks, which benefit from the improvement of simulation models. As reported in the literature reviews by Moodie (1988) and Birk (2006), many experimental fire tests were performed on pressure vessels in the last 50 years, providing valuable knowledge in the field. Based on these experiments, several models for the prediction of the response of pressurized tanks exposed to fire have been developed. Most of them (Aydemir et al., 1988; Birk, 1983; Bubbico and Mazzarotta, 2018; Dancer et al., 1990; Gong et al., 2004; Graves, 1973; Johnson, 1998a, 1998b; Scarponi et al., 2016; Yu et al., 1992) fall under the definition of “zone” models (also usually referred to as “integral” or “lumped” models), since they are based on the decomposition of the problem domain into one or more control volumes and on the solution of integral mass and heat balance equations for each of these volumes. Zone models such as AFFTAC (Johnson, 1998a, 1998b) and VessFire (Berge, 2009) are the current standard in transportation, process and oil&gas industry for the simulation of the response of tanks to fire exposure and for the assessment of the performance of thermal protection systems. Nevertheless, all the models belonging to this category rely to different extents on adjustable parameters and simplifying assumptions based on the analysis of experimental results. This limits their field of applicability to the range of experimental conditions adopted for their validation. Furthermore, most of them (including AFFTAC and VessFire) disregard key phenomena affecting the response of the fluid stored in the vessel, such as the thermal expansion of the liquid and the thermal stratification in the liquid and vapor phase (Scarponi et al., 2018).

Several authors succeeded in overcoming these limitations proposing CFD-based models. Shen et al., (2020) carried out a literature on recent applications of CFD to process safety and loss prevention, showing how such tools may provide new insights about industrial accident scenarios, improving their modelling and assisting the

design of mitigation measures such as fire protection systems. When discussing future research directions in domino effect assessment, Chen et al. (2020) indicate CFD-based models as candidates to accurately predict vulnerability of equipment items. However, due to the high computational cost, the first CFD approaches (D'Aulisa et al., 2014; Hadjisophocleous et al., 1990; Rum et al., 2018; Scarponi et al., 2018, 2019a) considered 2D domains only (usually a vertical section at the center of the tank). This excluded the possibility of simulating complex fire scenarios, such as partial engulfing pool fires or local jet fire impingement, where a variable fire load in the axial direction of the tank (for cylindrical tanks) is present. More recently, Scarponi et al. (2019b, 2020) were able to extend the analysis to the third dimension, proposing a CFD based modelling approach that was able to reproduce with good accuracy the full engulfing pool fire tests carried out by the Health and Safety Executive on LPG tanks of different sizes (Moodie et al., 1988, 1985). Nonetheless, a comprehensive validation of the CFD modelling approach proposed on fire scenarios different from full engulfing pool fires is still lacking.

The assessment of fire scenarios characterized by a non-uniform distribution of the heat load over the tank surface is particularly challenging. The effect of local phenomena, such as thermal stratification, free convective layer formation, strong temperature gradients between engulfed/not-engulfed zones producing thermal stresses, severely affect the overall conditions inside the tank and cannot be disregarded. Currently available lumped/zone models are not able to capture these complex phenomena and may produce non-conservative results when applied to partial fire engulfment scenarios. Furthermore, they do not allow for an accurate definition of non-uniform fire loads, such as those in which the flame only impacts one side of the storage tank. Examples of such scenarios occurred in the past are fire impingement due to jet fires (Birk et al., 2013), radiation form a nearby tank fire (Rum et al., 2018), and partially engulfing pool fires (Malm, 2018). Intense non-uniform fire loads are now becoming a relevant threat also for tank farms and isolated tanks installed in wildland-urban and wildland-industrial interface areas (Ricci et al., 2021; Scarponi et al., 2020), where severe wildfires may be experienced.

In the present study, the 3D CFD model originally proposed by Scarponi et al. (2019b) was further developed to allow the analysis of non-uniform fire scenarios. A thorough validation was carried out simulating a fire tests performed on a medium scale (1.9 m^3) LPG tank by Birk et al. (2006a), in which an array of liquid propane burners was used to reproduce partial pool fire engulfment conditions. As pointed out by several authors, pool fires are among the most dangerous category of industrial fires when domino effect is considered, due to their potential of escalation (Cozzani et al., 2016; Yi et al., 2020, 2019). CFD simulation results were analyzed in order to investigate how local flow field features promote thermal stratification, driving pressure build-up. A comparison to the results of a zone model was also carried out, evidencing the importance of specific phenomena not considered in these simplified models on overall operating parameters, such as tank internal pressure.

2 Description of the reference fire test experimental set up

The benchmark for the validation of the proposed CFD approach is an experimental fire test carried out by Birk and co-workers (Birk et al., 2006a). The test, referred to as "test 04-6" in the original experimental report (Birk et al., 2006a), was part of an experimental campaign aimed at studying the response of a medium scale (1.9 m^3) LPG tank to a partial engulfing fire (Birk et al., 2006a, 2006b). As shown in Figure 1, a cylindrical tank with hemispherical ends was used for the test, with an inner diameter of 0.953 m, a wall thickness of 7.1 mm and a total length (end to end) of 3.07 m. The fire was generated using a 5x5 array of liquid propane burners, designed to reproduce the heat load of an engulfing pool fire with a black body temperature in the range of 871 ± 56 °C. The burner system was set up so that the flame covered approximately the 25 % of the tank wall surface area (see Figure 1a). The test was the only one in the experimental campaign carried out without thermal protection and in favorable wind conditions, ensuring a quite constant contact between the flames and the tank (see Figure 1b). Thus, this test was considered as reference to assess the prediction capability of the modelling approach described in Section 3.

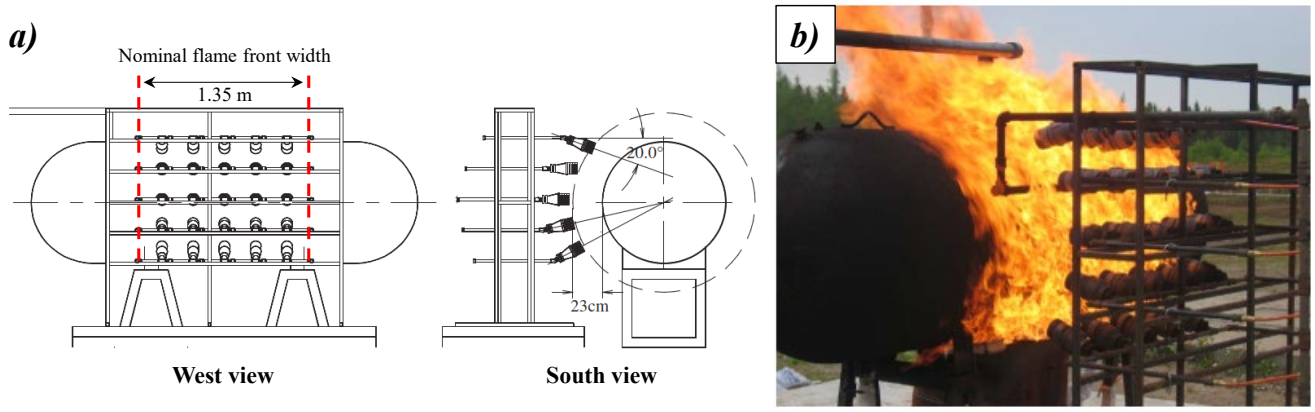

Figure 1: Burner array configuration (a) and experimental set-up (b). Adapted from Birk et al. (2006a).

Assuming that the heat flux entering the tank was entirely due to thermal radiation, a black body temperature of 866 °C was estimated by Birk et al. (2006a). The test tank was equipped with a static pressure transducer and 61 type K stainless-steel-sheathed lading thermocouples (with a 3 mm diameter), 48 of which were placed inside the tank to measure lading temperature (distributed over 5 vertical arrays, from I to V, see Figure 2) while 13 were fixed to the outer wall. A scheme illustrating the thermocouple positioning is reported in Figure 2.

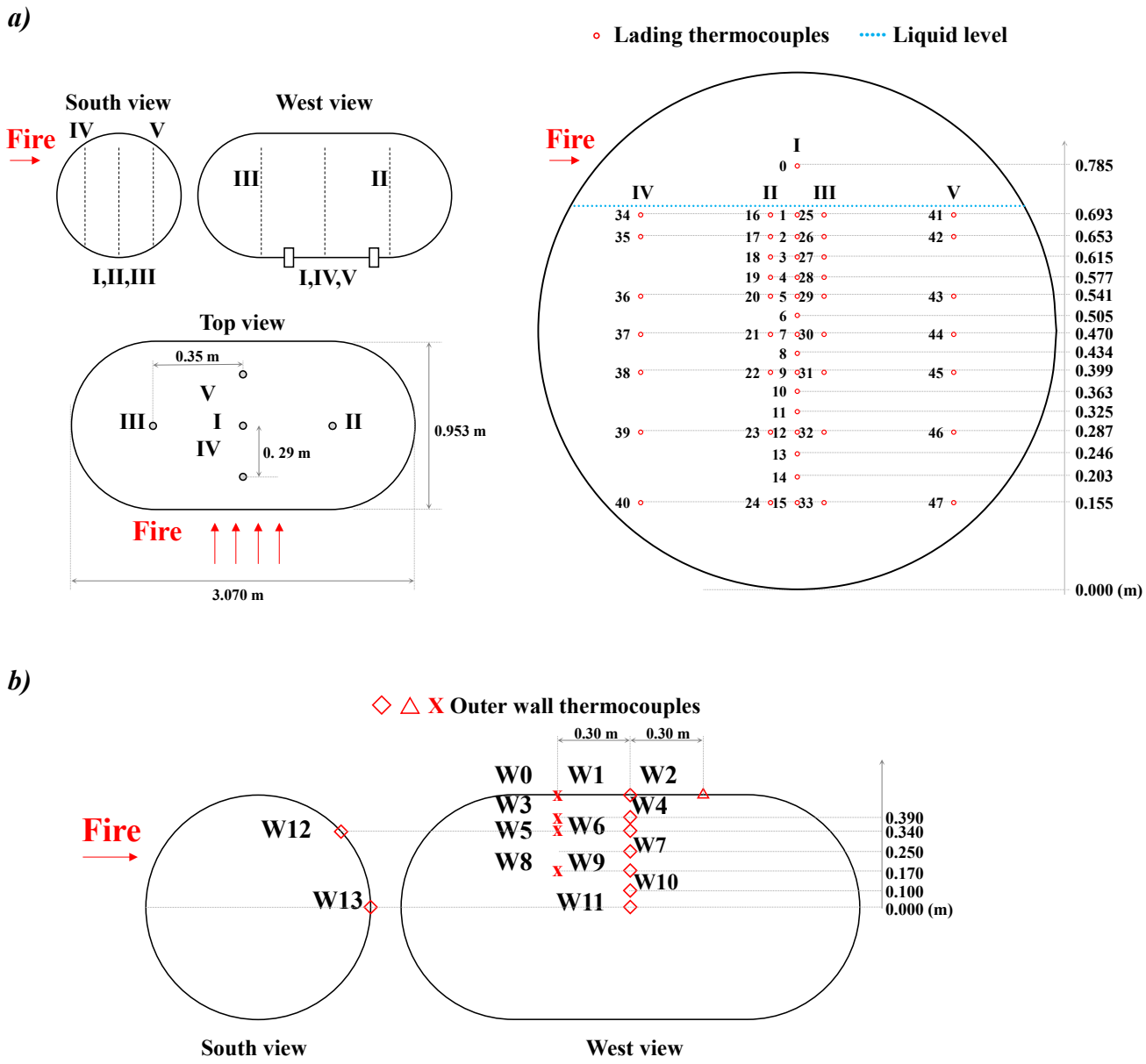

Figure 2: Scheme of thermocouples position in the lading (a) and on the outer wall (b). Thermocouples in the lading are distributed along the 5 vertical arrays (I to V) depicted in panel a.

Unfortunately, during the test taken as reference, data from thermocouples placed along the measuring array III (thermocouples 25 to 33) gave erroneous reading and were thus excluded from the present analysis.

The total duration of the test was 480s. The test was stopped right after a crack opened at the top of the tank. The initial liquid filling degree was 80 % by volume. The average lading and wall temperature at the beginning of the test were around 14 °C and 50 °C respectively. The quite high initial temperature of the wall was due to radiation from the sun. The initial pressure in the tank was 7.7 bar, which is about 0.6 bar higher than the vapor pressure of

pure propane at 14°C. This was caused by the initial temperature inhomogeneity and by impurities present in commercial propane, which was used in the test. More details on the experimental setup are reported elsewhere (Birk et al., 2006a, 2006b).

3 Numerical model

3.1 Governing equations

The starting point of the present study was the modelling setup proposed by Scarponi et al. (2019), that was modified in order to make it suitable for the simulation of the partial engulfment condition obtained during the fire test described in Section 2.

The model was implemented using ANSYS Fluent 18.2. The transport equations for mass, momentum, turbulence (k-ω SST model) and energy throughout the fluid (the tank lading) and the solid (the steel wall) domains are reported in Table 1. The Volume Of Fluid (VOF) (Hirt and Nichols, 1981), was adopted as multiphase model, which is suitable for simulating a system featuring two or more immiscible phases. Interphase mass transfer was reproduced using the evaporation-condensation model implemented in Fluent and based on the work of Hertz and Knudsen (Knudsen, 1934) (see E01 in Table 1). Thermal radiation inside the tank (i.e. radiation among points lying on the inner wall and between the inner wall and the fluid) was not modeled. The fluid in the tank was considered pure propane, with physical properties expressed as a function of temperature according to thermodynamic data provided in Liley et al., (1999). The vapor phase density was calculated using the Ideal Gas equation. This was preferred to the Soave-Redlich-Kwong used by Scarponi et al. (2019) to improve convergence. Simulations carried out in the modelling setup phase showed that the ideal gas equation resulted in slightly higher pressurization curves with respect to the Soave-Redlich-Kwong equation, with a maximum relative deviation always lower than 5%. Thermal conductivity, heat capacity and density of the tank wall, made of carbon steel, were taken from European standard EN 10222-1 (CEN - European Committee for Standardization, 1998).

At the beginning of the simulations, the tank lading was assumed to be motionless and at thermodynamic equilibrium (temperature 14°C, pressure 7.1 bar). In order to allow for a better comparison with experimental data, an offset of 0.6 bar was applied to pressure values obtained from CFD simulations, to compensate the discrepancy between the initial pressure in the fire test and the saturation pressure of pure propane at the initial temperature used in the CFD calculations, caused by the presence of impurities in the commercial propane used in the experimental test.

Table 1: Governing equation for the turbulent, two phases, transient CFD simulation developed.

ID	Property	Equations
E01	Volume fraction of the secondary phase (liquid)	$\frac{\partial}{\partial t}(\alpha_L \rho_L) + \nabla \cdot (\alpha_L \rho_L \vec{u}_L) = \dot{m}_{V\to L} - \dot{m}_{L\to V}$ ρ_L: liquid density; t: time; α_L: liquid volume fraction; $\vec{u}_L$: Reynolds averaged velocity; $m_{V\to L}$: and $m_{L\to V}$: condensation and evaporation liquid phase source terms, expressed as follows: $if\ T > T_{sat} \qquad m_{L\to V} = C_E \alpha_L \rho_L \left(\frac{T - T_{sat}}{T_{sat}}\right),\ m_{V\to L} = 0$ $if\ T < T_{sat} \qquad m_{L\to V} = 0, m_{V\to L} = C_C \alpha_V \rho_V \left(\frac{T_{sat} - T}{T_{sat}}\right)$ T: temperature; T_{sat}: saturation temperature; C_E and C_C: coefficients (both set to the default value of 0.1 s^{-1}); α_V: vapor volume fraction
E02	Volume fraction of the primary phase (vapor)	$\alpha_V = 1 - \alpha_L$
E03	Two-phase averaged quantity	$\varphi = \varphi_V \alpha_V + \varphi_L \alpha_L$ Two-phase volume fraction averaged property φ function of liquid and vapor properties (φ_L and φ_V, respectively) where φ can be density ρ, viscosity μ, turbulent viscosity μ_T, thermal conductivity k.
E04	Momentum	$\frac{\partial}{\partial t}(\rho \vec{u}) + \nabla \cdot (\rho \vec{u}\vec{u}) = -\nabla p + \nabla \cdot \left[\mu(\nabla \vec{u} + \nabla \vec{u}^T) - \frac{2}{3}\mu \nabla \cdot \vec{u} I\right] + \rho \vec{g} + \overrightarrow{F} - \nabla \cdot \tau'$ ρ: two-phase volume fraction averaged density; p: Reynolds averaged pressure; μ: two-phase averaged viscosity; g: gravity acceleration; I: identity tensor.
E05	Reynolds stress tensor (introducing the Boussinesq approximation)	$\tau' = \mu_T[(\nabla \vec{u} + \nabla \vec{u}^T)] - \frac{2}{3}(\rho K + \mu_T \nabla \cdot \vec{u} I)$ μ_T: two-phase averaged turbulent viscosity; K: turbulent kinetic energy
E06	Turbulent viscosity	$\mu_T = \frac{\rho K}{\omega}\frac{1}{L}$ ω: Turbulent specific dissipation rate; the definition of L can be found in (ANSYS inc, 2012)
E07	Turbulent kinetic energy	$\frac{\partial}{\partial t}(\rho K) + \nabla \cdot (\rho K \vec{u}) = \nabla \cdot (\Gamma_k \nabla K) + G_K - Y_K$ Γ_K: turbulent Prandtl number for K; G_K: generation of K due to mean velocity gradients; Y_K: dissipation of K due to turbulence. The definitions of Γ_K, G_K and Y_K can be found in (ANSYS inc, 2012)
E08	Turbulent specific dissipation rate	$\frac{\partial}{\partial t}(\rho \omega) + \nabla \cdot (\rho \omega \vec{u}) = \nabla \cdot (\Gamma_\omega \nabla \omega) + G_\omega - Y_\omega$ Γ_ω: turbulent Prandtl number for ω; G_ω: generation of ω; Y_ω: dissipation of ω. The definitions of Γ_ω, G_ω and Y_ω can be found in (ANSYS Inc, 2012)
E09	Energy (fluid domain)	$\frac{\partial}{\partial t}(\rho E) + \nabla \cdot \left(\vec{u}(\rho E + p)\right) = -\nabla p + \nabla \cdot \left[k_{eff} \nabla T\right] + \Delta H_{vap}(\dot{m}_{V\to L} - \dot{m}_{L\to V})$ E: two-phase Reynolds averaged specific energy; k_{eff}: effective thermal conductivity; ΔH_{vap}: heat of vaporization;
E10	Effective thermal conductivity	$k_{eff} = k + \frac{c_p \mu_T}{Pr_T}$ k = two-phase volume fraction averaged thermal conductivity c_p: two-phase volume fraction averaged heat capacity, Pr_T: turbulent Prandtl number = 0.85 (ANSYS Inc, 2012)
E11	Energy (solid domain)	$\frac{\partial}{\partial t}(\rho_s Cp_s T_s) = \nabla \cdot (k_s \nabla T_s)$ T_S: temperature in the solid; k_S: steel thermal conductivity; ρ_S steel density; Cp_S steel heat capacity

Turbulent kinetic energy and specific dissipation rate were initialized at 10^{-9} m^2/s^2 and 10^{-3} s^{-1} respectively. The no-slip condition was set at the inner wall whereas symmetry was assigned at the vertical plane cutting the tank in half (see Figure 3a).

A specific treatment was required for the definition of the thermal boundary condition on the outer wall of the tank. The aim was to reproduce the partial engulfment condition of the test. Only thermal radiation was considered as the heat transfer mechanism between the tank wall and the environment (flame and/or air). Under this assumption, the heat flux entering the faces of the cells laying on the external wall of the tank is calculated as follows:

$$q = \varepsilon_w (I_R - \sigma T_w^4) \quad (1)$$

where ε_w (assumed equal to 0.9, see Section 2) is the emissivity of the external wall, T_w is the temperature of the external wall, σ is the Stefan-Boltzmann constant (= $5.67 \cdot 10^{-8}$ W m^{-2} K^{-4}), and and I_R is the incident radiation on the tank wall. This can be calculated as follows from the black body temperature of the radiative source (T_R):

$$I_R = \sigma T_R^4 \quad (2)$$

The temperature of the radiative source varies according to whether the wall is in contact with the flame (in this case T_R is equal to the value of the flame black body temperature T_f) or with the air surrounding the tank (in this case T_R is equal to the value of the air temperature T_{air}). An intermediate zone is also included, in which the value I_R is obtained using a function combining T_f and T_{air}. This allowed reproducing the effect of the decay of thermal radiation between the portion of the wall engulfed in fire and the one in contact with the external air, as discussed in detail in Section 3.4.

The convective contribution to the heat transfer was excluded from the analysis in order to avoid the introduction of further uncertainties, due to the scarce confidence with which the convective heat transfer coefficient inside and outside the flame zone may be estimated. In the engulfed region, this assumption is supported by the limited contribution of convection, since the radiative contribution to the total heat transfer in liquid hydrocarbon pool fires is usually higher than 90% (Landucci et al., 2013). Furthermore, the estimation of the fire black body temperature (866 °C) provided in the experimental report was carried out assuming that the heat flux to the tank was entirely due to thermal radiation (see Section 2). Therefore, this value incorporates the convective heat transfer from the fire. Moreover, in the wall region in contact with air, the convective term is negative (heat is removed from the tank by the surrounding air). Therefore, from the process safety point of view, its exclusion from the analysis is a conservative assumption.

3.2 Solution methods

The following discretization schemes were considered: second order upwind for density, momentum, energy and turbulent quantities (k and ω), PRESTO! for pressure and Geo-Reconstruction for the phase volume fraction.

Pressure-velocity coupling was achieved using the SIMPLEC algorithm. Gradients were evaluated following the Least Square Cell-Based method.

A first order implicit scheme was adopted for the transient formulation, with a time step of 0.005 s.

At each time step, iteration was stopped when at least one of the residuals based convergence criteria (absolute or relative) reported in Table 2 were satisfied for all transport equations (see ANSYS Inc (2012) for more details). The simulations were run up to the time at which the internal pressure equalled the value at which the fire test was stopped (25.4 bar).

Table 2: Convergence criteria adopted in the present study.

Equation	Absolute criteria	Relative criteria
Continuity	10^{-4}	$5 \cdot 10^{-3}$
Momentum	10^{-4}	$5 \cdot 10^{-3}$
Energy	10^{-7}	$5 \cdot 10^{-3}$
k and ω	10^{-3}	$5 \cdot 10^{-2}$

3.3 Computational domain

Taking advantage of the symmetry of the problem (the engulfed region was centered with respect to the tank ends), only half of the tank was considered in the CFD simulation, as shown in Figure 3a. The computational domain (the tank solid wall and its internal volume, as shown in Figure 3b) was discretized using an unstructured grid obtained as a combination of tetrahedrons and hexahedrons with a maximum edge size of 3 cm (2 cm for the cells laying on the external wall). Appropriate resolution of the inner wall region, where the gradients of temperature and velocity are high, was achieved defining 25 inflation layers (volume growth rate of 1.1) with a first layer thickness of 0.2 mm (see Figure 3c). The resulting number of cells was 931,088. A grid independence study was successfully carried out generating a finer mesh featuring 4,792,991.

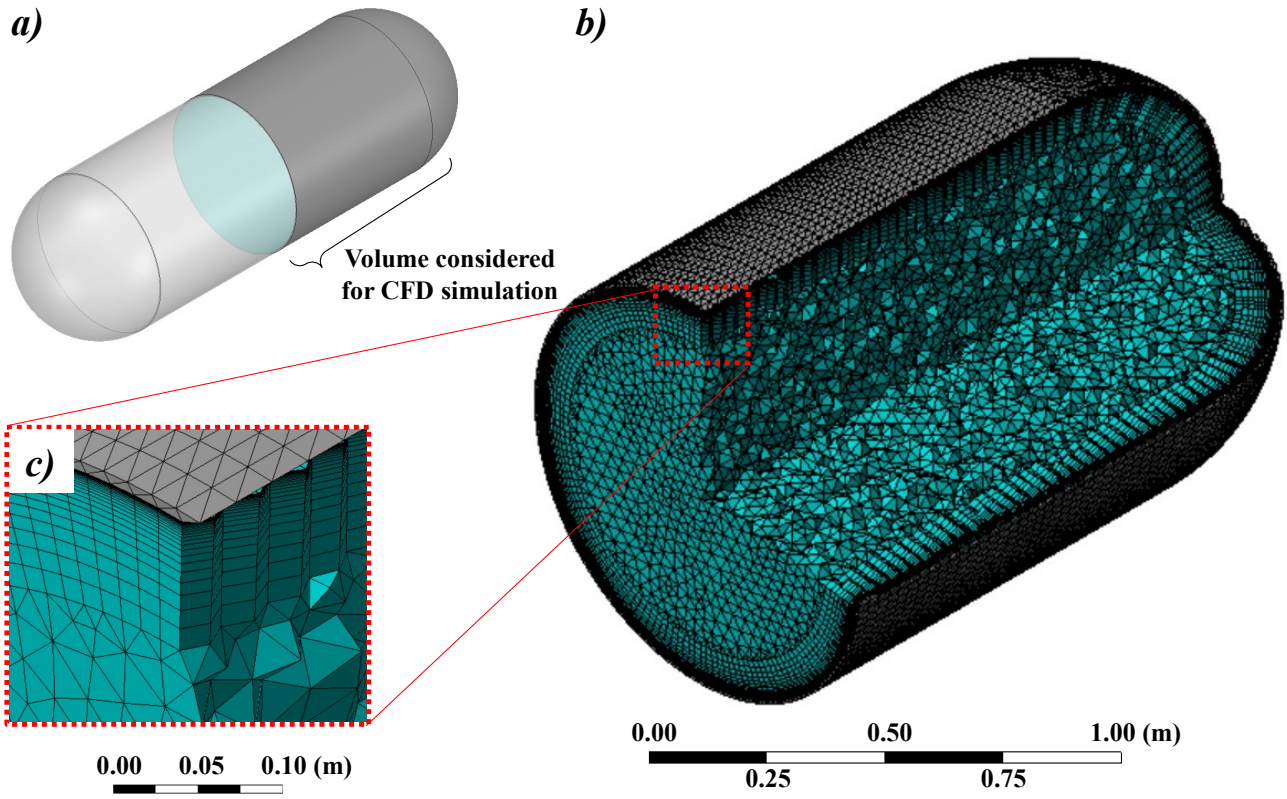

Figure 3: Tank portion considered for the CFD simulation (a); overview of the computational grid (b); (c) detail showing the increased grid resolution in the near wall region (cyan and gray cells refer to the fluid and the solid domains respectively).

3.4 Definition of the boundary conditions for partial engulfment

In order to simulate partial engulfment conditions, a space varying profile of the radiating temperature corresponding to the incident radiation on the tank outer wall was defined. As discussed in Section 3.1, three different zones, shown in Figure 4a, were considered.

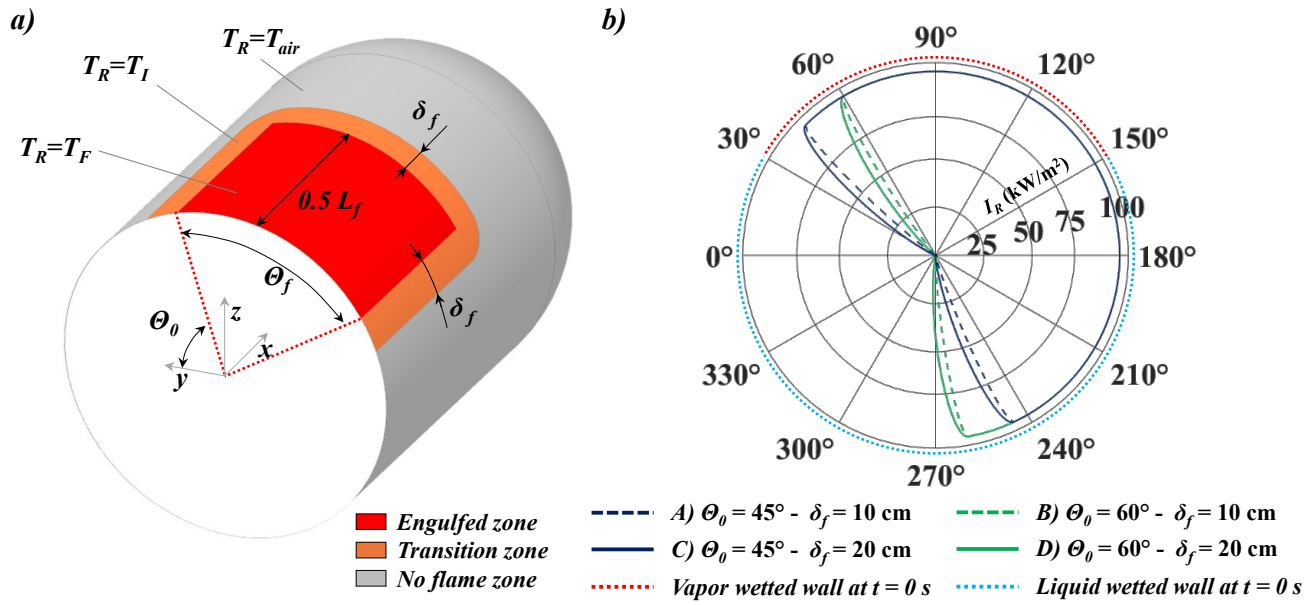

Figure 4: (a) Illustration of the 3 zones defined to reproduce partial engulfment conditions; (b) profiles of incident radiation as a function of the angular coordinate along the circumference at the center of the tank (i.e. the intersection of the tank outer wall with the symmetry plane) for the four simulation cases (A to D) defined in Table 3. Liquid and vapor wetted portions of the tank lading at the beginning of the simulations are identified by the cyan (liquid) and red (vapor) dotted lines.

The red zone in Figure 4a represents the engulfed region, defined in terms of the flame length along the tank axial direction (L_f) and the angle Θ_f. Here, a black body radiating temperature of 866 °C (estimated from experimental data, see Section 2), corresponding to an incident radiation (I_F) of 95.4 kW/m^2, was set as boundary condition. The liquid propane burners system was designed to provide a nominal value of L_f equal to 1.35 m (see Figure 1a) and to engulf the 25% of the tank surface. This implies that angle Θ_f in Figure 4a is equal to 200°. Concerning angle Θ_0 in Figure 4a, indicating the angular coordinate where the red zone begins, it was not possible to identify a single value from experimental data due to the variation of flame position. Therefore, two different cases were considered: Θ_0 = 45° and Θ_0 = 60°.

The grey zone in Figure 4a represents the region not impinged by the flame. A radiating temperature of 12°C (corresponding to the average ambient temperature measured during the test), corresponding to an incident radiation (I_{air}) of 0.4 kW/m^2, was set in this zone. Finally, in order to mimic the effect of the decay of thermal radiation between the red and the grey zones, an intermediate (or transition) zone was also included (orange zone in Figure 4a). In this zone, the incident radiation (I_I) decreases from a maximum value, the radiation of the flame at the border of the red zone, to a minimum value equal to the radiation coming from the environment surrounding the tank (at the border of the grey zone). In formulas, this is expressed as follows:

$$I_I = I_{air} + (I_F - I_{air}) \cdot \exp(-a \cdot \delta^2) \quad (3)$$

Where I_F is the incident radiation from the fire (95.4 kW/m^2), I_{air} incident radiation from the environment surrounding the tank (0.4 kW/m^2), δ is the distance from the border of the red zone and a is a parameter set so that when $\delta = \delta_F$ (see Figure 4a) the exponential in Eq. 3 is equal to 10^{-2}. Thus, the radiating temperature in the transition zone is obtained from I_I inverting Eq. 2. Despite the well controlled fire conditions during the test, it was not possible to obtain an accurate estimation of the extension of the transition zone as well as of the shape of the function describing the decay of thermal radiation between the engulfed zone and the region outside the flame. Furthermore, due to the limited number of thermocouples present on the outer wall, experimental data do not provide useful information to assess the extension and features of the transition zone. Thus, the decay of the thermal radiation between the engulfed zone and the region outside the flame was represented using the exponential function reported in Eq. 3. This ensures a smooth transition from I_F to I_{air}, supporting numerical convergence. On the other hand, due to the uncertainty in defining a single value for the extension of the transition zone δ_F (and/or for parameter a), two different situations were investigated: δ_F = 10 cm and δ_F = 20 cm. Thus, considering also the variation of Θ_0, a total of four simulations were run to validate the model, as shown in Table 3. Figure 4b shows the profiles of incident radiation as a function of the angular coordinate along the circumference at the center of the tank for each of the four simulations carried out.

Table 3: Values of Θ_0, Θ_f, δ_F and L_f used in the four simulation cases carried out for model validation

Simulation ID	$\boldsymbol{\Theta_0}$	$\boldsymbol{\delta_f}$	$\boldsymbol{\Theta_f}$	$\boldsymbol{L_f}$
A	45°	10 cm	200°	135 cm
B	60°	10 cm		
C	45°	20 cm		
D	60°	20 cm		

4 Results

4.1 Pressure build-up

The comparison between the pressurization curves obtained in the CFD simulations and the experimental data is reported in Figure 5.

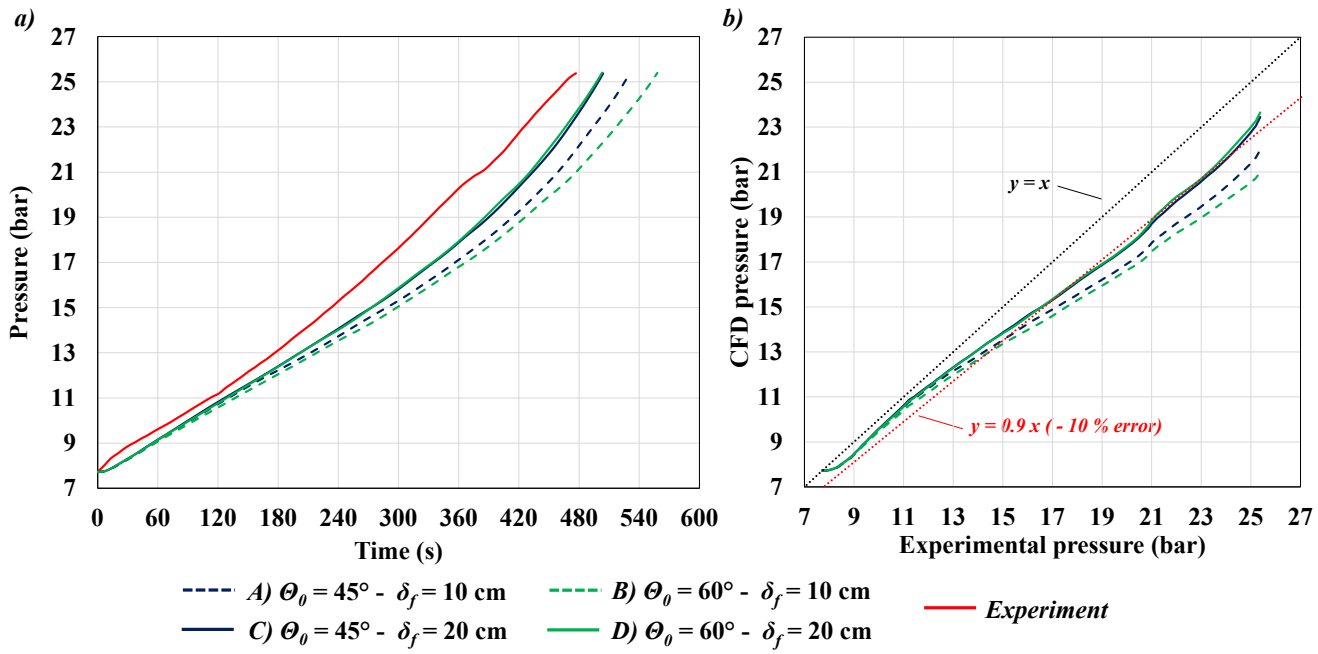

Figure 5: Comparison between the pressurization curves obtained in the four simulation cases defined in Table 3 and the experimental data: (a) pressure as a function of time; (b) parity plot showing simulated pressure values with respect to corresponding experimental data. An offset of 0.6 bar is applied to CFD results in order to match the initial pressure value measured in the fire test (see Section 2).

Pressure curves from simulation cases C and D (see Table 3), very close to each other, are in better agreement with experimental data with respect to cases A and B. Actually, in the first two cases (C and D), the relative deviation between the calculated and the measured pressure never exceeds 12% (with the curve for simulation case D showing a slightly better fit of experimental data), while maximum errors as high as 16% and 18% are recorded for cases A and B respectively. The maximum absolute difference of simulation results with respect to experimental data is of 3.7, 4.8, 2.5 and 2.3 bar for simulation cases A, B, C and D respectively. These results suggest that, within the range considered for each parameter, δ_F has a stronger influence on the pressurization rate than angle Θ_0. Furthermore, the experimental pressure curve is better matched by a higher value of δ_F (δ_F = 20 cm), regardless the value of Θ_0.

4.2 Lading Temperatures

The results of the analysis of the differences among the calculated and measured temperature values of the liquid are reported in Figure 6. In Figure 6a, for each of the 47 thermocouples measuring the liquid temperature and for each of the simulation cases described in Table 3, the value of $\Delta T_{i,max}$ is plotted versus the value of $\overline{\Delta T}_i$. The difference $\Delta T_{i,max}$ is the maximum difference between the calculated and measured temperature for the i-*th* thermocouple. The difference $\overline{\Delta T}_i$ is the average difference between the calculated and measured temperature for thermocouple *i*, calculated over the entire duration of the test (480 s) using a sampling interval of 1s. Due to the noisy reading of some of the thermocouples, experimental data have been smoothed considering a 10s moving mean.

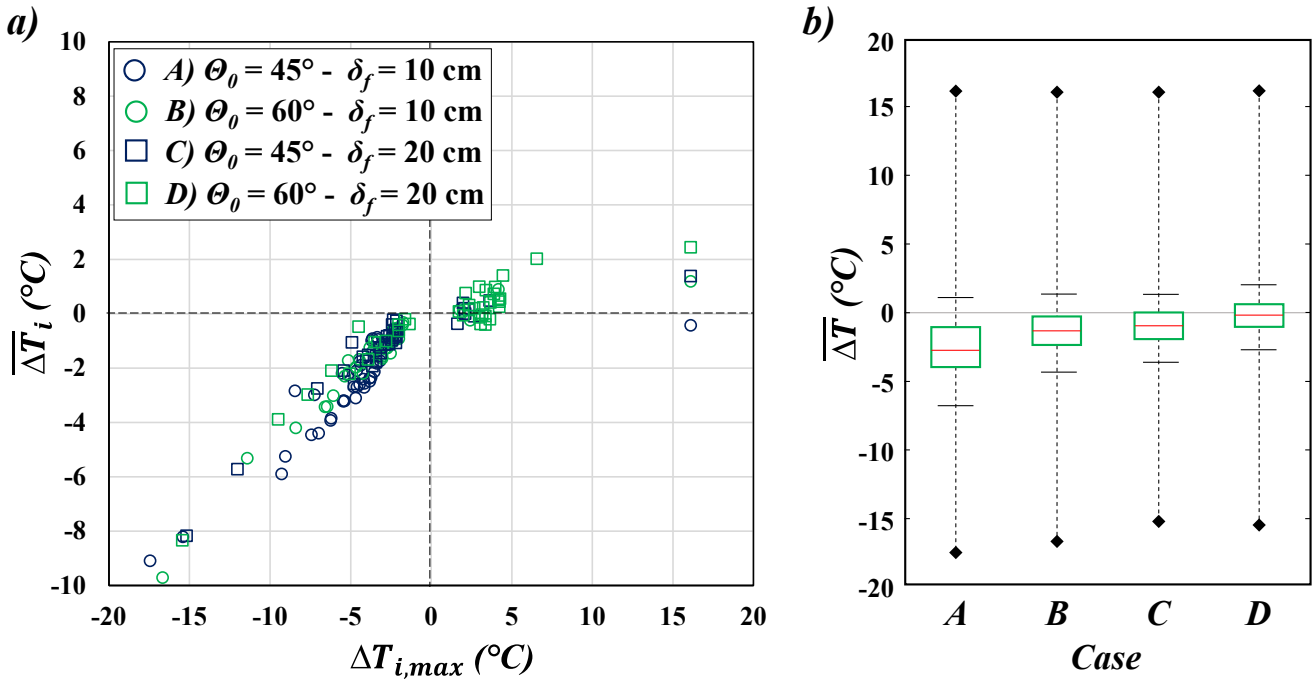

Figure 6: Comparison between calculated and measured liquid temperatures: (a) $\overline{\Delta T}_i$ vs. $\Delta T_{i,max}$ for all the thermocouples in the liquid phase; (b) distribution of the average deviation $\overline{\Delta T}$ obtained for simulation cases A, B, C and D (see Table 3). Red hyphens identify the mean of each distribution. Black hyphens are at a distance equal to the standard deviation from the mean of the distribution. Green boxes include the 2nd and the 3rd quartiles of the distributions. Black diamonds show the maximum and the minimum deviation from the experimental data.

Figure 6 clearly shows that $\Delta T_{i,max}$ falls within the interval the interval -19 to 16 °C, while and $\overline{\Delta T}_i$ is always between -10 and 15 ° C. For each of the simulation cases described in Table 3, Figure 6b provides a summary of

the error statistics showing the characteristics of the distribution of $\overline{\Delta T}$, defined as the difference between the calculated and measured temperature, evaluated for the entire set of thermocouples at intervals of 1 s. Also in the case of liquid temperatures, as for pressure data, the best match of CFD results with experimental measurements was obtained considering δ_F = 20 cm (simulation cases C and D). Thus, in the following, lading temperature profiles will be discussed only considering simulations cases C and D.

Figure 7 shows the comparison between temperatures from CFD simulations and experimental data for thermocouples placed along the vertical centerline of the tank (i.e. array I in Figure 2) at different time intervals since the beginning of the test. The results for the other thermocouple arrays are reported in the Supplementary Material (with the exclusion of data from array III, for which inconsistent measurements were recorded as mentioned in Section 2). As far as the temperatures of the liquid phase are concerned (i.e. the region outside the red shaded zone in Figure 7), CFD results reproduce the experimental data with good accuracy and limited differences are present among cases C and D. It is also possible to notice from the figure how the thermal stratification (the temperature difference between the bottom of the tank and the liquid-vapor interface) registered in the fire test is well replicated in CFD simulations. This is a very important aspect for the validation of the present modelling approach. Actually, several studies pointed out that, before Pressure Relieve Valve (PRV) opening, the pressurization of fired LPG tanks is driven by the temperature of the liquid-vapor interface (Aydemir et al., 1988; Leslie and Birk, 1991; Venart, 1999). It is therefore crucial, for a model aiming at accurately predicting pressure build up due to fire exposure, to be able to reproduce the vertical temperature gradient generated by free convective flows in the liquid phase. Such flows are three dimensional in nature and strongly dependent on the fire exposure mode. Hence, capturing such patters falls outside the modelling capabilities of the single and multi-zone lumped models commonly used in current practice by emergency responders and safety managers to predict fired tanks pressurization. The results shown in Figure 5 and Figure 7 demonstrate that this limitation can be overcome using a CFD based modelling approach as the one presented here, which is able to correctly capture the actual pressurization behavior of the tank, avoiding the underestimation that derives by neglecting the stratification phenomena, as discussed in Section 4.4.

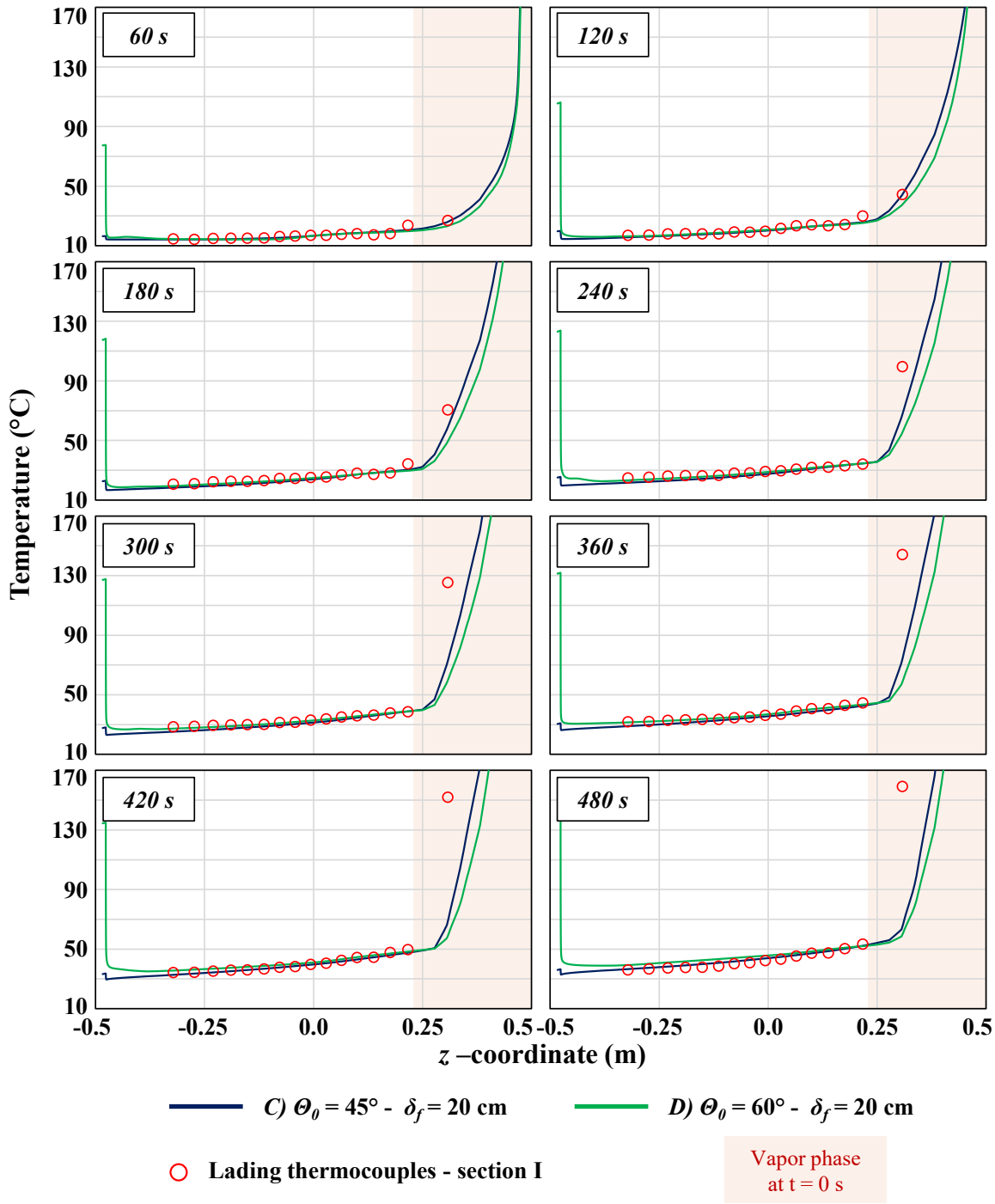

Figure 7: Comparison between experimental and CFD lading temperatures along array I (see Figure 2) at different instants of time for cases C and D. The red shaded zone represents the vapor phase at the beginning of the test. Note that the extension of this decreases during the test due to liquid expansion.

With respect to temperatures in the vapor phase, Figure 8 reports the comparison between CFD results and experimental data obtained from thermocouple 0 (Figure 2 shows the position of the thermocouple in the vapor

space). Figure 8a shows that after an initial time lapse (about 90s for simulation cases B and D, about 120s for simulation case C and about 150s for simulation case D) in which the CFD and experimental data are similar, the CFD results deviate considerably from the experimental data. A strong under prediction can be observed in all the cases following the initial time lapse. This behavior has two main causes. A first element is that thermal radiation inside the tank was not modelled. Actually, radiation from the inner tank wall would be partially absorbed by the vapor, increasing the temperature in the ullage. The second cause, probably the most relevant from the quantitative point of view, is the radiation error typically observed in gas temperature measurements in enclosures surrounded by hot walls (Carvalho and dos Santos, 1990), which may cause thermocouple to provide temperature values that are considerably different from the actual gas temperature (Daniels, 1968). The radiation error is known to increase with the increase of the wall temperature, explaining why the deviation between CFD results and experimental measurements becomes important only after a couple of minutes since the beginning of the test.

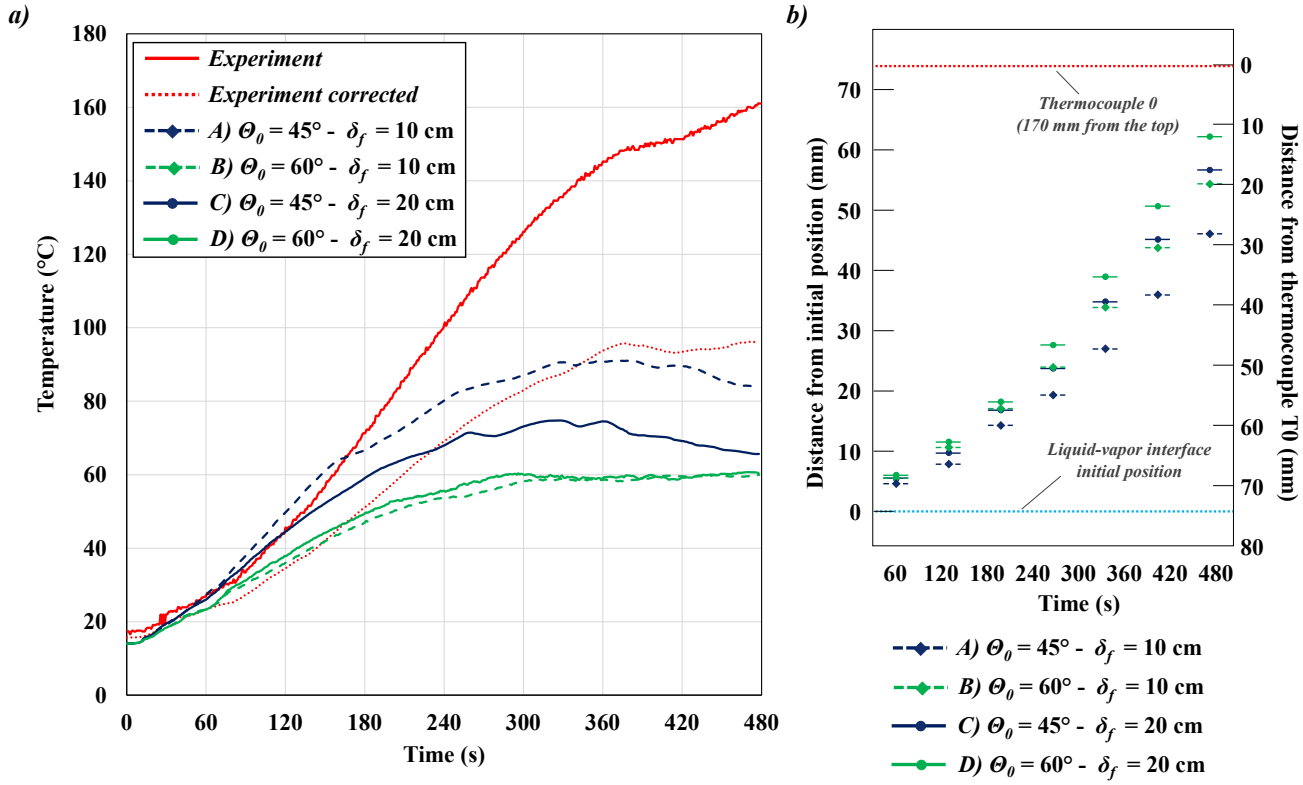

Figure 8: (a) Comparison between temperature values provided by thermocouple 0 and gas temperature obtained from the four simulation cases defined in Table 3. Experimental measurements corrected considering the radiation error are also reported (red dotted line); (b) Position of the vapour-liquid interface (identified as the vertical coordinate point where $\alpha_V = \alpha_L = 0.5$) with respect to time since the start of the fire calculated by CFD simulations.

Although a thorough radiation error analysis is outside the scope of the present study, an indicative estimation of the actual gas temperature was carried out following the procedure proposed by Brady and co workers (2015) and

was reported in Figure 8a (red dotted line). The details of the calculation of the radiation error are reported in the Supplementary Material. However, it should be remarked that the estimation of the temperature correction due to thermal radiation is based on a number of parameters that may be affected by strong uncertainty (Brady et al., 2015). This applies in particular to the emissivity of the thermocouple head and to the value of the Nusselt number used in the thermal balance. Thus, the corrected gas temperature shown in Figure 8a only represents a rough approximation of the actual temperature of the vapor space around thermocouple 0. Nevertheless, the corrected temperature shows a higher similarity to those obtained from CFD simulations than the original temperature reading.

When considering the differences among the simulation cases, Figure 8a shows that gas-phase temperatures obtained for cases A and C ($\Theta_0 = 45°$) are higher than those in cases B and D ($\Theta_0 = 60°$), since a higher amount of thermal energy enters directly into the vapor space when a lower value of Θ_0 is considered.

The comparison of results obtained in Case A and Case C (same value of Θ_0, higher value of δ_F in case C) stresses the importance of the strong cooling effect of the liquid-vapor interface on the vapor space. Figure 8b shows the transient evolution of the liquid-vapor interface position since the start of the fire in the different simulation cases. The interface position was identified as the vertical coordinate point where $\alpha_V = \alpha_L = 0.5$ (see E01 and E02 in Table 1). As shown in Figure 7, the thermal gradient above the interface is quite high, with values up to 15 K/cm. Therefore, even a small difference in the liquid-vapor interface position has a strong effect on the temperature value registered in the overhead region. Comparing the results reported in panels (a) and (b) of Figure 8, it is possible to observe that, as the level of the gas-liquid interface gradually raises, the slope of the curve showing the temperature increase with respect to time decreases, in coherence with experimental data. The higher values of the interface level obtained for case C results in lower gas-phase temperatures (up to 20°C) measured at the position of thermocouple 0.

4.3 Wall Temperatures

Figure 9 shows a comparison among the measured and calculated temperatures of the outer wall of the tank shell.

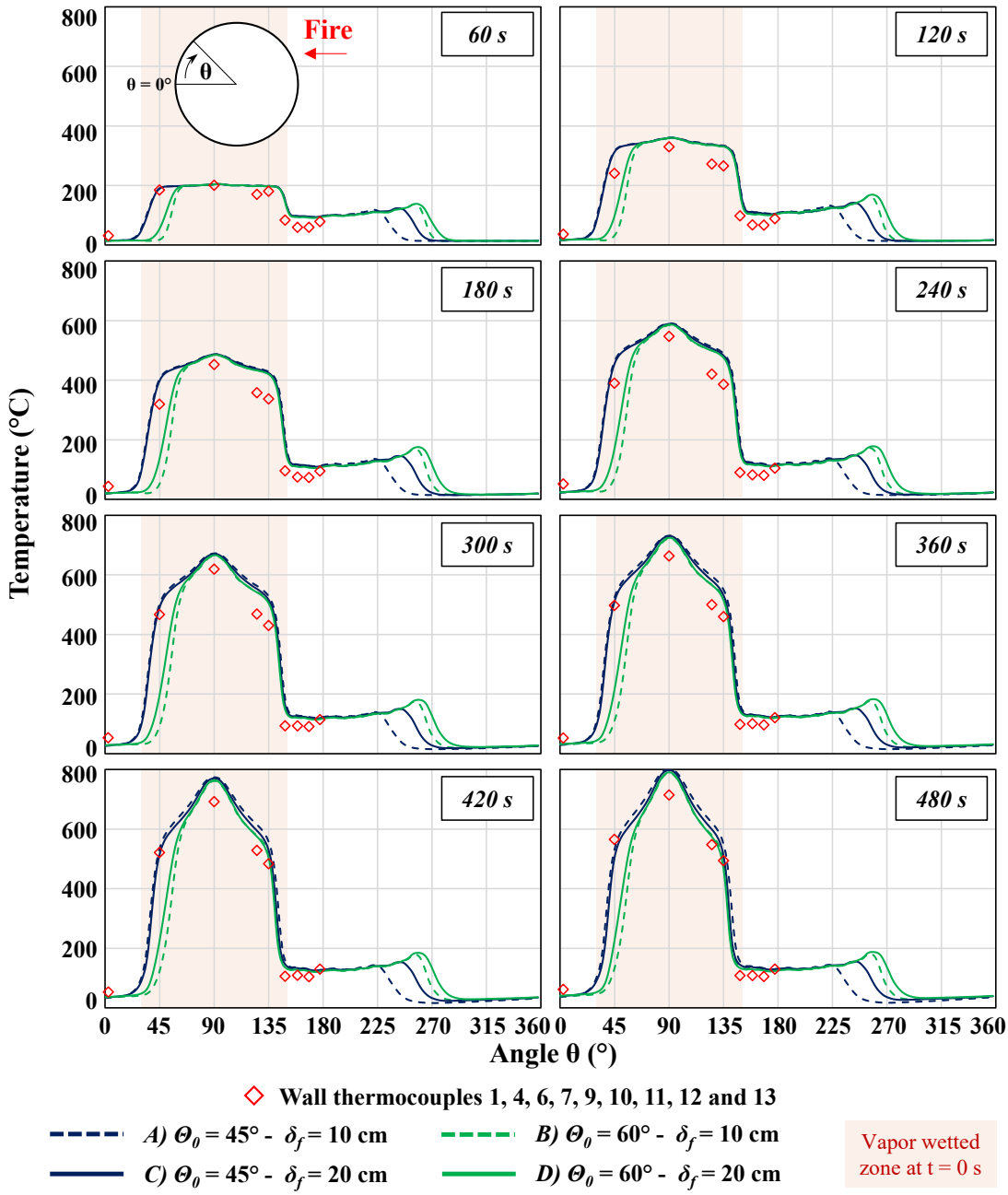

Figure 9: Comparison between simulated external wall temperature profiles at the central section of the tank and wall thermocouples measurements at different intervals of time since the start of the fire. The red shaded zone represents the portion of the wall in contact with the vapor at the beginning of the test, whose extension decreases during the test due to liquid expansion. Results obtained for the four simulation cases defined in Table 3 are shown.

The comparison between experimental data and CFD results shows a general good agreement for all the four simulations. In particular, the CFD model accurately reproduces the sharp temperature drop in correspondence with the liquid vapor interface (at the left and right sides of the red shaded zone highlighted in Figure 9). As observed in many other fire tests (see, for instance, Anderson et al., 1974 and Moodie et al., 1985), this drop is a consequence of the higher heat transfer coefficient in the liquid phase.

Focusing on wall thermocouple W12 (positioned at Θ = 45°), it is possible to observe that the experimental measurements are much better reproduced in the simulation cases assuming Θ_0 = 45° (i.e. cases A and C). This, together with similar observations made on pressurization curves and liquid phase temperature data, suggests that the thermal boundary condition assumed for case C in Table 3 (Θ_0 = 45° and δ_F = 20 cm) is that which approximates more accurately the actual fire exposure obtained in the experimental test. In all the cases (both simulations and test), the highest temperature is recorded at the top of the tank (Θ = 90 °C). Maximum temperature values are well beyond the value where thermal wakening of carbon steel becomes important (CEN - European Committee for Standardization, 1998). This explains the rupture pattern observed in the fire test: a crack formed at the top of the tank and propagated in the axial direction up to the limits of the engulfed area, stopping where the wall was colder (Birk et al. (2006a).

Overall, the CFD results shown in Figures 5, 7 and 9 provide a satisfactory simulation of the pressure and temperatures recorded during the experimental fire test. Thus, the CFD modelling approach proposed in the present study should be considered a reliable tool for the analysis of LPG tanks exposed to complex fire conditions such as partial engulfment.

4.4 Flow field and thermal stratification

As mentioned above, thermal stratification is a result of the local flow field characteristics, which determine the tank pressurization curve. Figure 10a shows a map of the vertical component of the velocity (u_z) at 60 s over the the horizontal plane passing through the center of the tank. Quite low values of u_z (- 0.05 < u_z < 0.05 m/s) can be observed all over the plane with the exception of the near wall region in correspondence with the engulfed zone (delimited by the red line), where the free convective layer stands out. Starting from a null value at the wall, u_z rises quickly (within few mm from the wall) reaching a maximum that oscillates (along the x-coordinate where the velocity peaks are varying with time) between 0.3 and 0.6 m/s and then falls back to an approximately zero value within about 4 cm from the wall. A fast drop of u_z is also visible moving from the border of the engulfed zone throughout the transition zone (i.e. moving from the red line to the orange one along the x-coordinate in Figure 10). Flow field characteristics similar to those just described are observed during the entire simulation. However, as time advances, the peaks in of u_z show progressively lower values and the oscillatory behavior along

the *x*-coordinate disappears. This can be observed in Figure 10b, showing the vertical velocities near the end of the simulation (480 s).

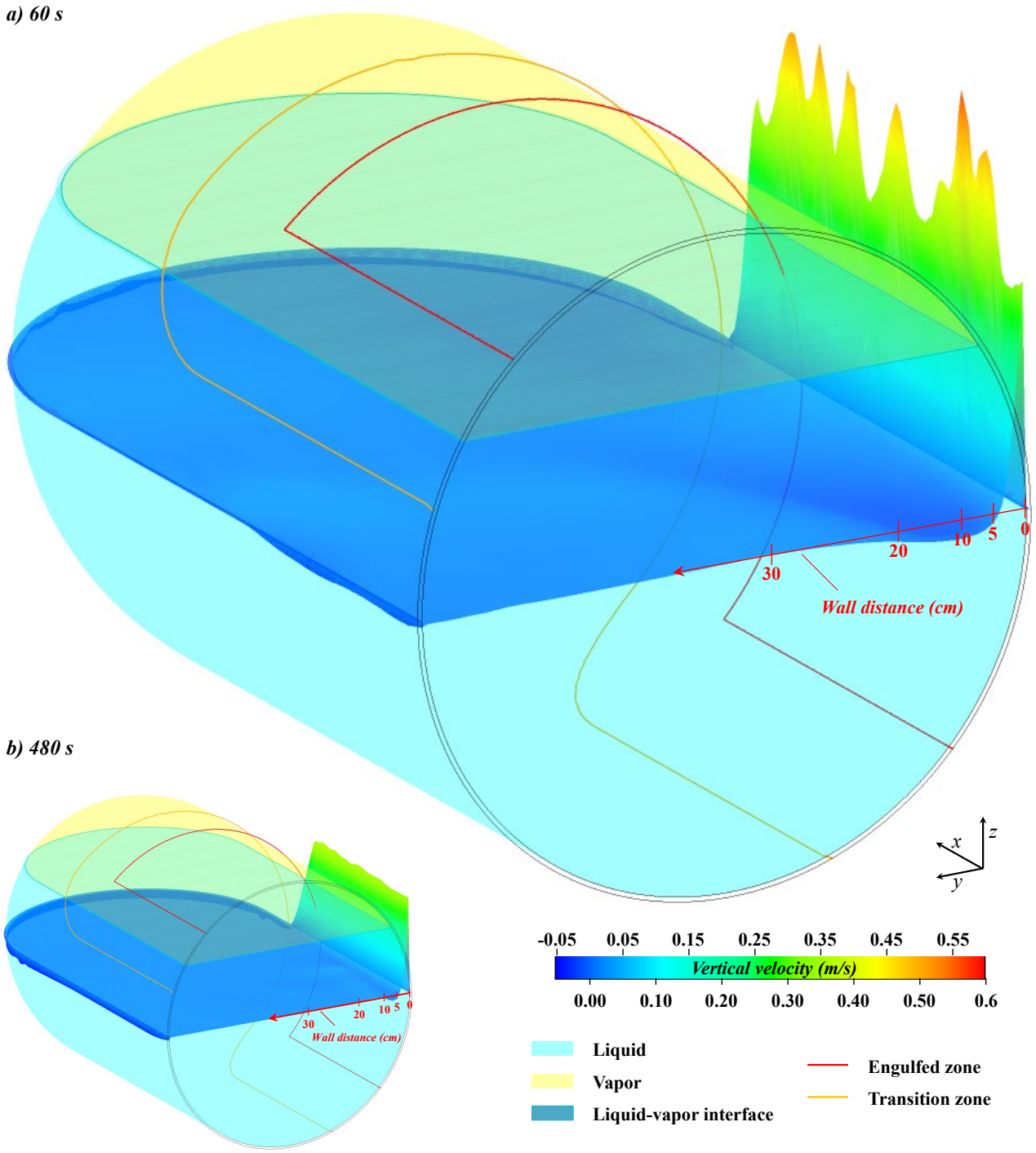

Figure 10: Map of the vertical component of the velocity (u_z) over the horizontal plane passign through the center of the tank (the contour surface was obtained by verticaly translating the the points on such plane by a distance proportional to the vertical velocity) after 60 s (a) and 480 s (b)

The peculiar characteristics of the free convective layer in correspondence with the engulfed zone determine a continuous intake of warm liquid that accumulates in the region beneath the liquid-vapor interface. This is clearly shown in Figure 11, reporting streamlines departing from the 10 black points highlighted in figure, which are equally spaced along a horizontal line (parallel to the tank axis), 1 cm away from the wall exposed to fire. Vectors composing each streamline are placed at an interval of 0.5 s to one another and extend for a total duration of 15 s. The yellow surface in Figure 11 cuts the liquid domain where the temperature equals the saturation temperature at the tank pressure ($T^*(p)$) reduced by 10 °C. Considering Figure 11a (120s after the start of the fire) it can be observed how the warm liquid in correspondence with the engulfed zone rises along the wall (also recalling liquid from outside the engulfed zone), follows a path parallel to the liquid-vapor interface and then deviates towards the tank end giving place to a recirculation cell. The flow field thus promotes the formation of a warm liquid layer (the region above the yellow surface is warmer than the one below), not limited to the area in the proximity of the engulfed zone, but extended beneath the entire liquid-vapor interface. A similar behavior is present in Figure 11b and c (respectively 240s and 360s after fire start). It is interesting to notice that the volume of the liquid featuring a temperature above $T^*(p) - 10\ °C$ is reduced when the time since the fire start is increased (e.g. compare Figure 11a (120 s) to Figure 11c (240 s)), confirming that the phenomenon of thermal stratification intensifies with time.

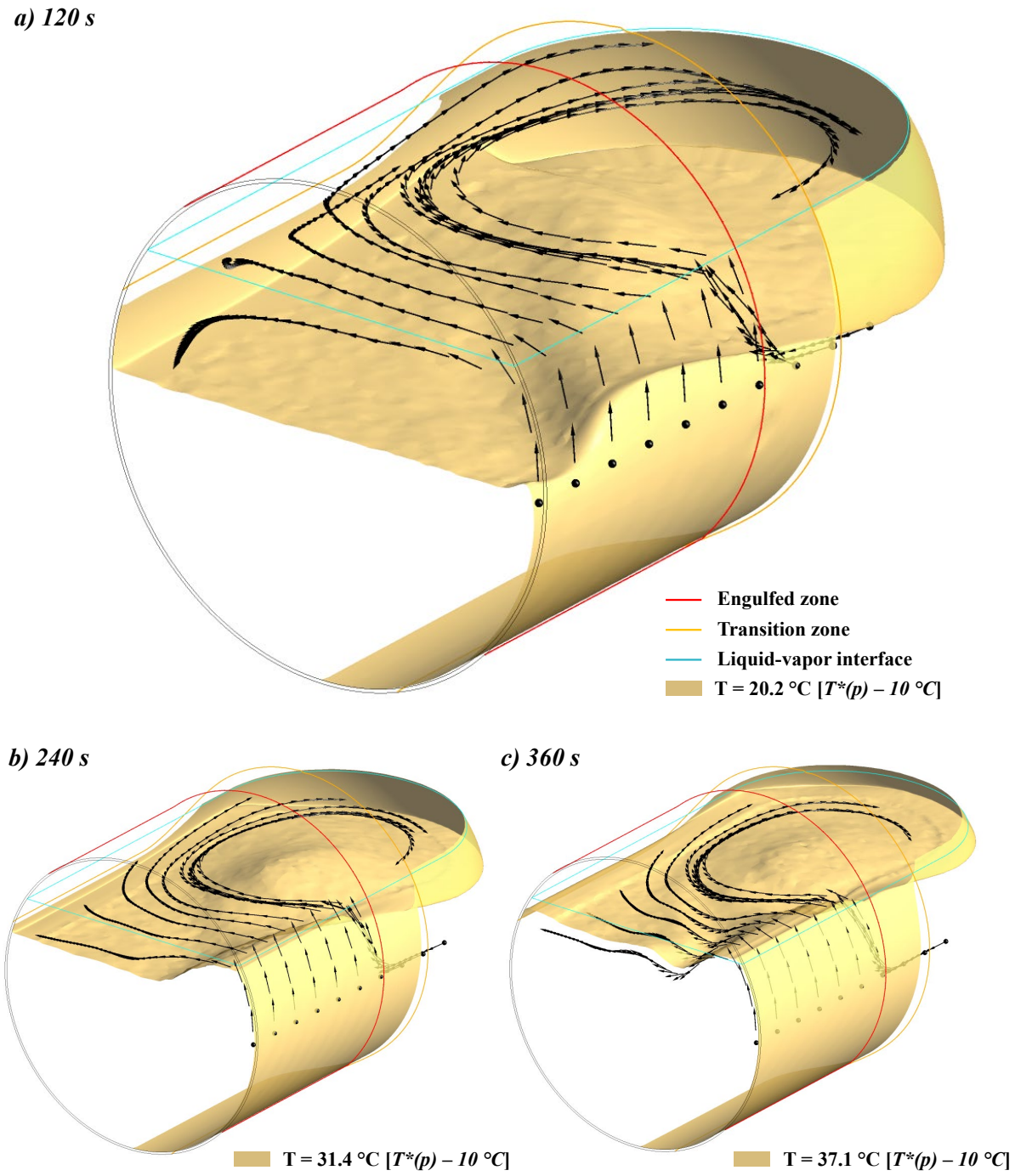

Figure 11: Streamlines departing from the 10 black points equally spaced along a horizontal line (parallel to the tank axis) at 1 cm from the wall exposed to fire at 120 (a), 240 (b) and 360 (c). Vectors composing each streamline are placed at an interval of 0.5 s to one another and extend for a total duration of 15 s. The yellow surface cuts the liquid domain where the temperature equals the saturation temperature at the tank pressure (T(p)) reduced by 10 °C.*

5 Discussion

The analysis of CFD results obtained in the simulation of the representative fire test selected proved that the modelling approach proposed is capable of reproducing experimental measurements for partial engulfment conditions with good accuracy. The parametric study of the geometrical features of the engulfed zone allowed identifying the boundary condition that better matches the fire exposure scenario obtained in the experiment. This highlights the importance of carefully designing fire systems in large-scale experimental tests, in order to achieve a good control of the fire shape and heat flux to the target. Thus, burners array should certainly be preferred to pool fires (obtained igniting a flammable liquid pool beneath the tank) in medium and large scale fire tests, due to the higher fire stability and therefore to the reproducibility of data. Actually, the well-defined and stable fire conditions achieved in the reference fire test selected allowed obtaining a satisfactory agreement between calculated and measured pressure curves. The same was obtained for wall and liquid temperatures, while an accurate comparison with experimental results was not possible for vapour phase temperature due to radiation error affecting experimental data.

The results obtained represent a step forward in modelling pressure vessels exposed to fire accident scenarios for the reasons discussed in the following. The CFD approach validated extends considerably the range of fire scenarios that can reliably be analysed, in particular considering the limits of lumped models used in current practice by emergency responders and risk analysts. In fact, none of such simplified models is nowadays able to predict, with a reasonable degree of confidence, the response of pressure vessels exposed to partially engulfing pool fires, jet fire impingement, and other fire scenarios featuring 3D characteristics (e.g. fireballs, or fire exposure in the presence of defective thermal insulation, wildfire fronts at the wildland-urban and wildland industrial interface). Actually, they do not allow the user to accurately specify complex fire loads. In perspective, the results obtained may be used for the training of such models in order to extend their prediction capabilities to account, at least by a conservative approach, for these scenarios.

This aspect is of particular importance since zone or lumped models currently used in design and emergency planning, being not able to capture stratification phenomena as those discussed in Section 4.4, may provide under-conservative results. An example is reported in Figure 12, where the results provided by the CFD simulation of case C (see Table 3) are compared to those obtained by the simulation of the experimental test using a zone model, RADMOD. Details on how the RADMOD simulation was carried out are reported in the Supplementary Material. The RADMOD zone model, developed by Cozzani and coworkers (Cozzani et al., 2006; Gubinelli, 2005), was applied in several studies to calculate the time to failure of tanks exposed to fire radiation (e.g. see Khakzad, 2019; Landucci et al., 2009; Ricci et al., 2021).

Figure 12a reports the difference between the pressure in the tank (p) and the saturation pressure calculated at the average liquid temperature ($p^*(T_{L\_ave})$), while Figure 12b reports the difference between the average liquid

temperature (T_{L_ave}) and the saturation temperature calculated at the tank pressure ($T^*(p)$), obtained using the CFD model. Both curves represent a measure of thermal stratification. The pressure curve shows that the pressure builds up much faster than the saturation pressure at the average liquid temperature. The temperature curve increases continuously up to a value of around 21°C, showing that most of the liquid phase deviates considerably from equilibrium conditions towards a subcooled state.

Figure 12b also shows the difference between CFD and RADMOD results in terms of average liquid temperature (blue dotted line) and tank pressure (red dotted line). The average liquid temperature calculated by the two models is almost the same (the blue dotted line never exceeds 1 °C), while the difference in the prediction of tank pressurization is evident, and becomes equal to more than 8 bar at the end of the simulation. In the RADMOD model, the tank pressure corresponds to the saturation pressure calculated at the liquid temperature. Thus, the results of the above comparison suggest that both modelling approaches accurately predict the amount of thermal energy transferred from the fire to the liquid phase, but only the CFD model is able to reproduce the pressurization curve measured during the experiment.

The inability of the zone model in capturing thermal stratification leads to the under-conservative results shown in Figure 12a. The zone model provides a relevant under-prediction of the pressure in the tank when compared to experimental data. The time to reach 25.4 bar, the maximum pressure value recorded in the experimental test, is about 1.7 times higher when using the zone model.

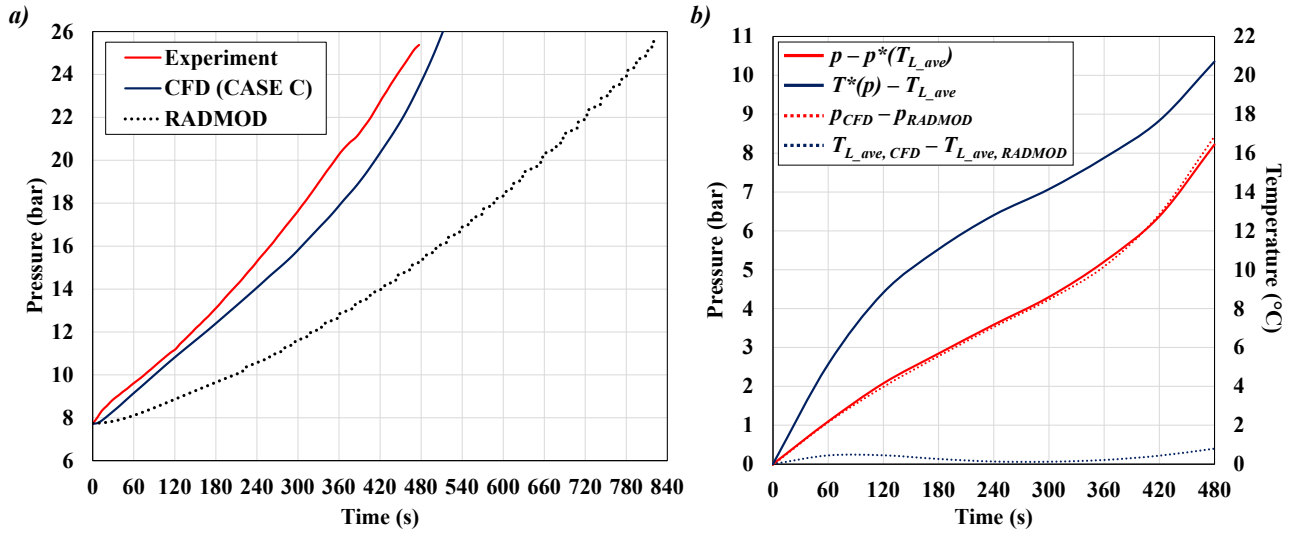

Figure 12: (a) Comparison of experimental results for pressure versus time obtained in the experimental test to CFD simulations (Case C in Table 3) and RADMOD zone model results; (b) Effect of thermal stratification on key operating parameters of the vessel exposed to fire in the experimental test simulated: differences between i) the average liquid temperature T_{L_ave} and the saturation temperature calculated at the tank pressure $T^*(p)$ obtained from CFD simulations (Case C); ii) the pressure in the tank, p, and the saturation pressure of pure propane calculated at the average liquid temperature, $p^*(T_{L\_ave})$; iii) the pressure obtained from CFD and RADMOD simulations of the experimental test; and iv) the average liquid temperature obtained from CFD and RADMOD simulations of the experimental test.

The CFD approach developed resulted in a robust and validated tool for the study of the key phenomena driving pressure build-up due to fire exposure in real-size vessels, limiting the need for full-scale fire tests, which are expensive, time consuming and pose relevant safety and environmental issues. In this perspective, the analysis reported in Sections 4.3 represents an example of how the CFD modelling approach may be considered as a "digital twin" of a fire test, and can be used to investigate in detail the internal flow field generated as a consequence of local fire exposure, affecting heat propagation throughout the tank and determining its rate of pressurization.

The safety of pressurized vessels would undoubtedly benefit from the application of the model to a parametric analysis aimed at assessing the effects of different fire exposure modes, heat fluxes, filling degrees and tank geometries on the thermo-fluid dynamic response of the tank. In perspective, the CFD model may also be used as a virtual workbench to test the effectiveness of thermal protection systems. For instance, simulations may be run to estimate the minimum thickness of thermal insulation required to ensure tank integrity. CFD simulations may as well support the design of water mist systems, indicating the most effective disposition of nozzles and their optimum flow rate. In addition, a reliable estimation of the pressurization rate generated by a specific fire scenario may be useful to ensure a correct PRV sizing and to estimate depressurization time in process and storage vessels. More in general, the model may drive improvements in the design of pressurized vessels and safety systems, increasing the safety of storage and transportation operations, as well as emergency response planning.

Among the drawbacks of the CFD approach, the computational time stands out. On an Intel® Core™ i9-9940 CPU @ 3.30GHz (simulations were carried in parallel on 16 logical processors), it took approximately 30 min to simulate 1s real time. The simulation of the entire test took approximately 10 days. Considering that the computational domain in the present study was limited to half of the tank volume (thanks to the symmetric nature of the problem), and that real-size storage and transportation tanks have much wider volumes than the tank used in the reference fire test, the modelling approach considered at the state is not adequate if a quick assessment of tank response is needed. This issue will possibly be solved in the future, although transient solutions as the training of surrogate models or the extension of the existing lumped models by empirical add-ons are advisable for the management of emergency planning and process safety issues.

In perspective, further problems still need to be thoroughly explored: the performance of defective thermal insulation (see for instance the studies carried out by Yoon and Birk (2004) and Scarponi et al. (2017)) and, mostly, the fluid behaviour after the opening of the PRV. Additional research is needed also to address the integration of fluid-dynamic simulations with the stress analysis of the tank, aiming at a more detailed and less conservative approach in the prediction of tank failure (Manu et al., (2009)). Pressure rise data and transient wall temperature maps form CFD simulations may be used as time and space varying boundary condition for finite element analysis, with the aim of accurately reproducing the mechanical and thermal stresses in the tank walls. The results of such analysis may provide new insights on the rupture pattern of tanks under fire exposure.

6 Conclusions

The availability of models for the prediction of the behavior of pressurized tanks under fire exposure is a key element to improve the design of tanks and of fire protection systems. Robustness and accuracy of such models are essential requirements, since they are applied to process and transportation safety. These features pass through the model ability to reproduce the basic physical phenomena underlying tank heat up and pressurization. A CFD modelling approach previously validated against full engulfing pool fire tests was validated in the present study to simulate partial engulfment conditions. The detailed comparison of pressure build-up, lading temperature and wall temperature predictions with the results of an experimental fire test proved the ability of the model in capturing the complex phenomena leading to thermal stratification of the liquid and fast pressurization. This confirms that the CFD model developed is a reliable tool for the simulation of pressure tanks under fire exposure also when complex fire conditions, such as partial engulfment, are considered. In perspective, this allows for the simulation of fire scenarios where lumped/zone models currently used may provide under-conservative results.

Moreover, the CFD model developed allows investigating key phenomena occurring at local scale, that are hard (if not impossible) to analyze during experimental fire tests. These results thus represent a valuable source of information, which may drive improvements in vessel design and increase the safety of storage and transportation operations, reducing the need for expensive and time-consuming full-scale fire tests.

7 References

Abbasi, T., Abbasi, S.A., 2007. The boiling liquid expanding vapour explosion (BLEVE): mechanism, consequence assessment, management. J. Hazard. Mater. 141, 489–519. https://doi.org/10.1016/j.jhazmat.2006.09.056

Anderson, C., Townsend, W., Zook, J., Cowgill, G., 1974. The effects of a fire environment on a rail tank car filled with LPG. US Dept Trans.Rept No FRA-OR&D 31–75.

Aydemir, N.U., Magapu, V.K., Sousa, A.C.M., Venart, J.E.S., 1988. Thermal response analysis of LPG tanks exposed to fire. J. Hazard. Mater. 20, 239–262. https://doi.org/10.1016/0304-3894(88)87015-8

Berge, G., 2009. Verification of VessFire.

Birk, A.M., Dusserre, G., Heymes, F., 2013. Analysis of a propane sphere BLEVE. Chem. Eng. Trans. 31, 481–486.

Birk, A.M., 2006. Fire Testing and Computer Modelling of Rail Tank-Cars Engulfed in Fires: Literature Review.

Birk, A.M., 1983. Development and validation of a mathematical model of a rail tank-car engulfed in fire. Dev. Valid. a Math. Model a Rail Tank-car Engulfed Fire PhD Thesis. Queen's University, Kingston, Ontario, Canada.

Birk, A.M., Poirier, D., Davison, C., 2006a. On the response of 500 gal propane tanks to a 25% engulfing fire. J. Loss Prev. Process Ind. 19, 527–541. https://doi.org/10.1016/j.jlp.2005.12.008

Birk, A.M., Poirier, D., Davison, C., 2006b. On the thermal rupture of 1.9 m3 propane pressure vessels with defects in their thermal protection system. J. Loss Prev. Process Ind. 19, 582–597. https://doi.org/10.1016/j.jlp.2006.02.006

Bradley, I., Scarponi, G.E., Otremba, F., Birk, A.M., 2021. An overview of test standards and regulations relevant to the fire testing of pressure vessels. Process Saf. Environ. Prot. 145, 150–156. https://doi.org/10.1016/j.psep.2020.07.047

Brady, K.B., Hui, X., Sung, C.-J., Niemeyer, K.E., 2015. Counterflow ignition of n-butanol at atmospheric and elevated pressures. Combust. Flame 162, 3596–3611. https://doi.org/https://doi.org/10.1016/j.combustflame.2015.06.017

Bubbico, R., Mazzarotta, B., 2018. Dynamic response of a tank containing liquefied gas under pressure exposed to a fire: A simplified model. Process Saf. Environ. Prot. 113, 242–254. https://doi.org/10.1016/j.psep.2017.10.016

Carvalho, J.A., dos Santos, W.F.N., 1990. Radiation errors in temperature measurements with thermocouples in a cylindrical combustor. Int. Commun. Heat Mass Transf. 17, 663–673. https://doi.org/https://doi.org/10.1016/0735-1933(90)90014-B

CEN - European Committee for Standardization, 1998. EN 10222-1. Steel forgings for pressure purposes. Part 1: General requirements for open die forgings. European Committee for Standardization, Brussels, Belgium.

Chen, C., Reniers, G., Khakzad, N., 2020. A thorough classification and discussion of approaches for modeling and managing domino effects in the process industries. Saf. Sci. 125, 104618. https://doi.org/10.1016/j.ssci.2020.104618

Cozzani, V., Gubinelli, G., Salzano, E., 2006. Escalation thresholds in the assessment of domino accidental events. J. Hazard. Mater. 129, 1–21. https://doi.org/10.1016/j.jhazmat.2005.08.012

D'Aulisa A., Tugnoli A., Cozzani, V., Landucci, G., Birk, A.M., D'Aulisa, A., Tugnoli, A., Cozzani, V., Landucci, G., Birk, A.M., 2014. CFD modeling of LPG vessels under fire exposure conditions. AIChE J. 60, 4292–4305. https://doi.org/10.1002/aic.14599

Dancer, D., Sallet, D.W., Germany, W., 1990. Pressure and temperature response of liquefied gases in containers and pressure vessels which are subjected to accidental heat input. J. Hazard. Mater. 25, 3–18. https://doi.org/10.1016/0304-3894(90)85066-C

Daniels, G.E., 1968. Measurement of Gas Temperature and the Radiation Compensating Thermocouple. J. Appl. Meteorol. 7, 1026–1035. https://doi.org/10.1175/1520-0450(1968)007<1026:MOGTAT>2.0.CO;2

Di Padova, A., Tugnoli, A., Cozzani, V., Barbaresi, T., Tallone, F., 2011. Identification of fireproofing zones in Oil&Gas facilities by a risk-based procedure. J. Hazard. Mater. 191, 83–93.

https://doi.org/10.1016/j.jhazmat.2011.04.043

Gong, Y.W., Lin, W.S., Gu, A.Z., Lu, X.S., 2004. A simplified model to predict the thermal response of PLG and its influence on BLEVE. J. Hazard. Mater. 108, 21–26. https://doi.org/10.1016/j.jhazmat.2004.01.012

Graves, K.W., 1973. Development of a Computer Model for Modeling the Heat Effects on a Tank Car. US Department of Transportation, Federal Railroad Administration, Washington DC.

Gubinelli, G., 2005. Domino effect in the process industries: quantitative methodologies for the evaluation of consequences. Ph. D. thesis in Chemical Engineering, University of Pisa, Pisa.

Hadjisophocleous, G. V, Sousa, A.C.M., Venart, J.E.S., 1990. A study of the effect of the tank diameter on the thermal stratification in LPG tanks subjected to fire engulfment. J. Hazard. Mater. 25, 19–31.

inc, A., 2012. ANSYS® FLUENT® 14.5 Theory Guide. ANSYS Inc, Cecil Township, PA.

Johnson, M.R., 1998a. Tank Car Thermal Analysis, Volume 1, User's Manual for Analysis Program. Department of Transportation, Federal Railroad Administration, Washington DC.

Johnson, M.R., 1998b. Tank Car Thermal Analysis, Volume 2, Technical Documentation Report for Analysis Program. US Department of Transportation, Federal Railroad Administration, Washington DC.

Khakzad, N., 2019. Modeling wildfire spread in wildland-industrial interfaces using dynamic Bayesian network. Reliab. Eng. Syst. Saf. 189, 165–176. https://doi.org/10.1016/j.ress.2019.04.006

Knudsen, M., 1934. The kinetic theory of gases. Some modern aspects. Methuen and Co., Ltd, London, UK.

Landucci, G., Cozzani, V., Birk, M., 2013. Heat Radiation Effects, Domino Effects in the Process Industries: Modelling, Prevention and Managing. Elsevier, Amsterdam, The Netherlands.

Landucci, G., Gubinelli, G., Antonioni, G., Cozzani, V., 2009. The assessment of the damage probability of storage tanks in domino events triggered by fire. Accid. Anal. Prev. 41, 1206–1215. https://doi.org/10.1016/j.aap.2008.05.006

Leslie, I.R.M., Birk, A.M., 1991. State of the art review of pressure liquefied gas container failure modes and associated projectile hazards. J. Hazard. Mater. https://doi.org/10.1016/0304-3894(91)87083-E

Malm, S., 2018. New CCTV shows moment gas tanker plowed into back of a truck, sparking explosion that left one dead and scores injured in Italy. MailOnline.

Manu, C.C., Birk, A.M., Kim, I.Y., 2009. Stress rupture predictions of pressure vessels exposed to fully engulfing and local impingement accidental fire heat loads. Eng. Fail. Anal. 16, 1141–1152.

Mcdevitt, C.A., 1990. Initiation step of boiling liquid expanding vapor ezplosions. J. Hazard. Mater. 25, 169–180.

Moodie, K., 1988. Experiment and modelling:- an overiview with particular reference to fire engulfment. J. Hazard. Mater. 20, 149–175. https://doi.org/10.1016/0304-3894(88)87011-0

Moodie, K., Billinge, K., Cutler, D.P., 1985. The fire engulfment of LPG storage tanks. IChemE Symp. Ser. No. 93 87–106.

Moodie, K., Cowley, L.T.T., Denny, R.B.B., Small, L.M.M., Williams, I., 1988. Fire engulfment tests on a 5 tonne

LPG tank. J. Hazard. Mater. 20, 55–71. https://doi.org/10.1016/0304-3894(88)87006-7

Ricci, F., Scarponi, G.E., Pastor, E., Planas, E., Cozzani, V., 2021. Safety distances for storage tanks to prevent fire damage in Wildland-Industrial Interface 147, 693–702. https://doi.org/10.1016/j.psep.2021.01.002

Rum, A., Landucci, G., Galletti, C., 2018. Coupling of integral methods and CFD for modeling complex industrial accidents. J. Loss Prev. Process Ind. 53, 115–128. https://doi.org/10.1016/j.jlp.2017.09.006

Scarponi, G.E., Landucci, G., Birk, A.M., Cozzani, V., 2019a. CFD Study of the Fire Response of Vessels Containing Liquefied Gases. Chem. Eng. Trans. 77, 373–378. https://doi.org/10.3303/CET1977063

Scarponi, G.E., Landucci, G., Birk, A.M., Cozzani, V., 2018. LPG vessels exposed to fire: Scale effects on pressure build-up. J. Loss Prev. Process Ind. 56, 342–358. https://doi.org/10.1016/J.JLP.2018.09.015

Scarponi, G.E., Landucci, G., Birk, A.M.A.M., Cozzani, V., 2019b. An innovative three-dimensional approach for the simulation of pressure vessels exposed to fire. J. Loss Prev. Process Ind. 61, 160–173. https://doi.org/10.1016/j.jlp.2019.06.008

Scarponi, G.E., Landucci, G., Ovidi, F., Cozzani, V., 2016. Lumped model for the assessment of the thermal and mechanical response of LNG tanks exposed to fire. Chem. Eng. Trans. 53, 307–312. https://doi.org/10.3303/CET1653052

Scarponi, G.E., Landucci, G., Tugnoli, A., Cozzani, V., Birk, A.M., 2017. Performance assessment of thermal protection coatings of hazardous material tankers in the presence of defects. Process Saf. Environ. Prot. 105, 393–409. https://doi.org/10.1016/j.psep.2016.10.009

Scarponi, G.E., Pastor, E., Planas, E., Cozzani, V., 2020. Analysis of the impact of wildland-urban-interface fires on LPG domestic tanks. Saf. Sci. 124, 104588. https://doi.org/10.1016/j.ssci.2019.104588

Shen, R., Jiao, Z., Parker, T., Sun, Y., Wang, Q., 2020. Recent application of Computational Fluid Dynamics (CFD) in process safety and loss prevention: A review. J. Loss Prev. Process Ind. 67, 104252. https://doi.org/10.1016/j.jlp.2020.104252

Tugnoli, A., Cozzani, V., Di Padova, A., Barbaresi, T., Tallone, F., 2012. Mitigation of fire damage and escalation by fireproofing: A risk-based strategy. Reliab. Eng. Syst. Saf. 105, 25–35. https://doi.org/10.1016/j.ress.2011.11.002

U.S. Department of Transportation, 2013. Lac-Mégantic railroad accident discussion and DOT safety recommendations. Report 4910-06-P. Washington, DC.

Venart, J.E.S.E.S., 1999. Boiling Liquid Expanding Vapor Explosions (BLEVE): Possible Failure Mechanisms. ASTM Spec. Tech. Publ. 1336, 112–134.

Yi, H., Feng, Y., Park, H., Wang, Q., 2020. Configuration predictions of large liquefied petroleum gas (LPG) pool fires using CFD method. J. Loss Prev. Process Ind. 65, 104099. https://doi.org/10.1016/j.jlp.2020.104099

Yi, H., Feng, Y., Wang, Q., 2019. Computational fluid dynamics (CFD) study of heat radiation from large liquefied petroleum gas (LPG) pool fires. J. Loss Prev. Process Ind. 61, 262–274.

https://doi.org/10.1016/j.jlp.2019.06.015

Yoon, K.T., Birk, A.M., 2004. Computational Fluid Dynamics Analysis of Local Heating of Propane Tanks.

Yu, C.M., Aydemir, N.U., Venart, J.E.S., 1992. Transient free convection and thermal stratification in uniformly-heated partially-filled horizontal cylindrical and spherical vessels. J. Therm. Sci. 1, 114–122.